Flow of wet powder in a conical centrifugal filter - An analytical model

A.F.M. Bizard and D.D. Symons
Cambridge University Engineering Department
October 29, 2010

Abstract

A one-dimensional analytical model is developed for the steady state, axisymmetric, slender flow of saturated powder in a rotating perforated cone. Both the powder and the fluid spin with the cone without relative slip in the hoop direction. They migrate up the wall of the cone along a generator under centrifugal force, which also forces the fluid out of the cone through the powder layer and the porous wall. The input mixture thus evolves from a saturated paste at inlet into a nearly dry powder at outlet. The powder is treated as incompressible, and its motion depends only upon the forces applied at its external boundaries: its constitutive model is irrelevant. Surface tension effects are assumed negligible compared to the centrifugal acceleration. Two models are considered for the flow structure at inlet: Fully settled powder at inlet or hindered settling of an initially homogeneous slurry. The position of the colour line is similar for these two models, dominant dimensionless groups are identified who control the position of the colour line in a continuous conical centrifuge.

1 Introduction

Centrifugal filters are commonly used in the food processing and chemical industries in order to separate the liquid and solid phases of a mixture, where the two phases have comparable densities. There exist two main types of centrifugal filter: *batch* machines with a cylindrical basket and *continuous* machines with a conical basket. The present study is a continuation of the work initiated in (Bizard, Symons & Fleck 2010) and focuses on continuous conical centrifuges. A typical application of the conical centrifuge is the separation of liquid molasses from sugar crystals in the sugar industry. The rotating basket of the machine spins at about 1000 rpm and comprises a cone with a jump in cone angle along its length: a lower impervious cone has a semi-angle of $\alpha = 15°$ whereas the upper perforated cone has α=30°, see Fig.1.

[Figure 1 about here.]

The outlet diameter at the top of the upper cone is on the order of 1m. The inside wall of the upper, perforated cone is fitted with a slotted screen, thereby allowing for fluid drainage but preventing powder losses. The feedstock, in the form of a sugar/molasses slurry, of liquid volume fraction 50% and temperature 60°C, is introduced along the spin axis into the lower impervious cone at a constant flow rate. The slurry acquires the angular velocity of the basket and migrates up the wall of the lower cone into the upper, perforated cone. At this stage the slurry can either have started separating into two phases, a saturated powder layer and a fluid layer, or be still an homogeneous fluid loaded with particles (Region A in Fig.2). In this analysis we shall consider two extreme cases: in a first model all the particles are settled before the flow reaches the inlet of the perforated cone; in a second model the flow is still a homogeneous slurry. The actual flow behaviour is expected to be somewhere between these two extremes, but we will show that the difference in position of the colour line is small, so that the considered cases give a good representation of the behaviour of the flow in a conical centrifugal filter with the advantage of being significantly simpler than a more complete analysis. Liquid seepage gets the slurry to quickly evolve into a 2-phase flow, the top of which is damp while the bottom is still saturated with liquid. This region, Region B in Fig.2, is commonly called the colour line in the sugar industry. It usually starts at about a third of the cone and spans over 10-20cm. Final drainage as well as washing operations occur in region C. Thus, a continuous conical centrifuge should be designed in order to maximize the time spent by the crystals in region C. This time depends upon the distance between the colour line and the top lip as well as the crystal velocity in this region, which was found constant in (Bizard et al. 2010).

In the current study we analyse the successive states through which the material evolves within the cone. We consider the case where the particles are denser than the fluid, so that they settle on the wall instead of floating on top of the fluid. The friction law presented in (Bizard et al. 2010) is modified to take buoyancy into account in states A and B. Liquid drainage in damp powder is minor and such powder is therefore treated as a homogeneous continuous medium of constant properties.

A major objective of the analysis is to explore the sensitivity of the residence time of crystals in region C to operating conditions, through the two following outputs: position of the colour line, and flow velocity.

[Figure 2 about here.]

[Figure 3 about here.]

1.1 Review of past experimental results and analysis on the flow of saturated powder in a rotating perforated cone.

Continuous centrifuges are mainly used in the sugar industry. Swindells (Swindells 1982) and Greig (Greig 1995) have extensively studied these machines in a semi-empirical fashion. While their work provides valuable insight in the operation of conical centrifuges it lacks the fundamental understanding of the underlying mechanics, which makes their results difficult to transpose to other applications. This study will aim at completing this, relying on their experimental results to assess the validity of a theoretical approach.

1.1.1 Fluid velocity before the colour line

The flow of a Newtonian fluid in a rotating impervious cone has been studied by Makarytchev et al (Makarytchev, Xue, Langrish & Prince 1997). They conclude, like Bizard et al (Bizard et al. 2010), that the through-thickness velocity profile of a slender flow is nearly parabolic and its velocity is controlled by the equilibrium between the basal shear traction and the weight of the fluid only. In such conditions the influence of outlet and inlet boundary conditions is negligible at a rather short distance from the boundaries.

1.1.2 Velocity after the colour line

When studying the flow of cane sugar massecuite in a laboratory-scale machine, Swindells finds that the flow velocity in the upper part of the cone, past the colour line, is essentially constant around 0.1m.s^{-1}. This is consistent with the residence time of 10s generally obtained in industrial machines of about 1m length along the generatrix, and with the theoretical result of (Bizard et al. 2010), which will be developed further in this work.

1.1.3 Friction at the wall

In an attempt to obtain an analytical model for continuous centrifuges, Swindells (Swindells 1982) assumes that the shear traction at the wall past the colour line is pure Coulomb friction, and explains the uniform velocity mentioned earlier by a strict equality between the coefficient of friction of the powder/wall interface, b, and the cone slope $\tan\alpha$. Observations by Swindells support the idea that Coulomb friction dominates the shear traction at the wall: if the cone angle is more than a few degrees smaller or larger than the Coulomb friction coefficient b the machine does not work properly. While we acknowledge the importance

of Coulomb friction at the wall interface, we have shown (Bizard et al. 2010) that this configuration is highly unstable under high gravity. In such conditions the particles would either stick to the wall or leave the basket at high velocity. Liquid drainage ensures constant renewal of a thin liquid film at the powder/wall interface, and shearing of this film generates a velocity-dependent shear traction in addition to the Coulomb friction term, as developed in (Bizard et al. 2010). Shear traction at the wall τ then writes

$$\tau = au + bp_{eff} \tag{1}$$

where a is a constant friction parameter and p_{eff} the interfacial effective pressure between the crystals and the wall. Yilmazer et al (Yilmazer & Kalyon 1989) performed experiments on powder saturated with Newtonian fluid and obtained a as

$$a = \frac{8\mu}{D} \tag{2}$$

where μ is the intersticial fluid viscosity and D the particle average size. We will use this result in this work. We note that while friction law (1) is relevant for all regions A,B and C of the cone as shown in Fig.3 the relative amplitude of its terms is likely to depend upon the moisture content: In region A, the small difference in solid and fluid density implies a low effective pressure, so that the Coulomb friction term could be neglected. On the contrary in region C, Coulomb friction is expected to dominate as mentioned above, and while the velocity-dependent term is necessary to ensure flow stability its amplitude is expected to be smaller than that of the Coulomb friction term. Region B will be a transition region, where buoyancy effects vanish rapidly and thereby enhance the effective pressure.
For completeness we note that the coefficient a as given by (2) is only valid when the interface particles are immerged in liquid, so that this relation does not apply to region C, where a decreases due to the reduction in liquid content at the interface. We will however assume that the drain heigt as defined by (Dombrowski & Brownell 1954) is of the same order of magnitude as the mean crystal size, so that a is in region C on the same order of magnitude as the value given by (2) for regions A and B.

1.1.4 Drainage

Dombrowski and Brownell (Dombrowski & Brownell 1954) present a simple model for a settled powder/liquid mixture under vertical downwards gravitational acceleration g.

They divide the thickness in two layers: the top layer is damp at a moisture ratio M_0 while the bottom layer is saturated. The transition thickness between these two layers is vanishingly thin. While the relative thickness of each layer depend on time, they find that the moisture content of the top layer only depends upon the dimensionless capillary number N_{CAP}, defined as

$$N_{CAP} = \frac{k_p \rho_f g}{\gamma} \tag{3}$$

where k_p is the powder permeability, ρ_f the liquid density and γ the fluid surface tension. The angle of contact between the fluid surface and the particles is taken as 0.
Dombrowski and Brownell find that for $N_{CAP} < 10^{-2}$ M_0 is independent of N_{CAP}, while it decreases exponentially when N_{CAP} exceeds 10^{-2}. These results have several implications for continuous conical centrifuges:

- The vanishing transition thickness between the damp layer for which the saturation is minimal at S_0 and the saturated layer is a strong indication that the moisture content of damp powder in a centrifuge does not depend upon time but rather upon N_{CAP}.

- As long as region C exists in the cone, the drying efficiency of the machine will not be improved by an increase in size unless the outer radius is so large that N_{CAP} exceeds 10^{-2}, in which case any subsequent size increase will significantly improve the dryness of the powder at outlet.

1.1.5 Screen resistance to flow

The screen resistance to flow depends upon the Reynolds number within a slot. If viscous effects are dominant, a Poiseuille plane flow model would be appropriate, if the inertial effects dominate, a model using Bernoulli's theorem will be more adequate. In this work we will assume a large predominance of the viscous effects, so that the volumetric flow rate per unit area q is related to the pressure gradient dp/dz through the screen via:

$$q = \frac{k_s}{\mu} \frac{dp}{dz} \tag{4}$$

where k_s is the screen permeability. If the slots are significantly deeper than wide k_s can be estimated via

$$k_s = \frac{n_s w^2}{12} \tag{5}$$

where n_s is the screen open area and w the slots width. While industrial screens slots commonly have an increasing width, as shown in Fig.4, and should therefore have a permeability lower than that predicted by (5), we will use this result as a conservative estimate of the screen permeability. Note that the permeability measured by Swindells (Swindells 1982) is on the same order of magnitude as that predicted by (5) for practical values of n_s and w. In the case of a flow under gravity g normal to a screen of thickness h_s, (4) can be re-written as

$$q = \frac{k_s}{\mu} \frac{\rho_f g h_s + \Delta p}{h_s} \tag{6}$$

where Δp is the pressure difference across the screen.

[Figure 4 about here.]

1.1.6 Slurry viscosity

In the second model for region A we will consider the flow of slurry, mixture of liquid and solid particles. (Oliver & Ward 1953) found experimentally that when the solid mass ratio of a slurry does not exceed 30%, the mixture can still be taken as Newtonian, its viscosity depending upon the solid mass ratio. For the particular case of sugar massecuite, (Rouillard & Koenig 1980) showed that for high solid mass ratios (up to 0.6) the mixture can still be treated as Newtonian viscous within a practical range of shear rates, the viscosity increasing exponentially with the solid content. We will show that the viscosity of the slurry has only a mild influence on the position of the colour line in a continuous centrifuge, so that considering more complex models such as the power-law viscous model presented by (Swindells 1982) is unnecessary.

1.2 Outline of paper

A one dimensional analysis is now given for the flow of a solid/liquid mixture within a rotating perforated cone. The analysis assumes that the flow is thin (i.e. that the thickness of the powder, or fluid, layer is much less than the inner radius of the basket), and that both the gravitational and Coriolis components of acceleration are negligible compared to the centrifugal action. These assumptions match the conditions observed in the practical case of a conical centrifuge as used in the sugar industry. Two models are considered for the flow in region A. In a first model the particles are all settled before reaching the perforated cone and a layer of pure fluid flows on top of a saturated powder layer. In a second model

the slurry is assumed to be homogeneous, with no initial settling of powder, at inlet. In the perforated cone seepage drags the particles down onto the wall and a powder layer builds up gradually. The remaining slurry flows on top of it and while its thickness decreases through drainage, its moisture content remains at its initial value.
Equilibrium and mass conservation relations are established for each of the regions described in Fig.3. Ordinary differential equations (ODEs) are obtained for the flow in regions A and B and an algebraic equation, idependent of the coordiante r, is obtained for the flow velocity in region C.
Key non-dimensional groups are identified and conditions to maximize the crystals residence time in region C are given.

2 Problem statement

Consider the steady state laminar flow of a thin layer within a spinning cone, of apex angle 2α and constant spin speed Ω, as shown in Fig.5.

[Figure 5 about here.]

Introduce the spherical co-ordinates (r, θ, ϕ) in an Eulerian reference frame, and assume that the fluid has the same circumferential speed (in the ϕ-direction) as the cone at any radius r, as observed in the practical operation of a conical centrifuge. Ω is sufficiently large for the acceleration due to gravity to be negligible compared to $r\Omega^2 \sin\alpha$ at any radius r. Write $v(r, \theta)$ as the radial component of the fluid velocity. We shall simplify the problem by introducing $u(r)$ as the mean value of $v(r, \theta)$ over the thickness $h(r)$ of the thin layer, where the radial velocity $u(r)$ is much less than the circumferential velocity $r\Omega \sin\alpha$ for any radius r. Likewise, the Cauchy stress on a fluid element averaged over its thickness has components $(\sigma_r, \sigma_\theta, \sigma_\phi, \tau_{r\theta})$ which depend only upon r. The wall traction in the r-direction has a normal component $p(r)$ and a shear component $\tau(r)$.

The fluid is treated as incompressible, Newtonian,with a density ρ_f, dynamic viscosity μ and surface tension γ. The powder is also treated as incompressible, with a density ρ_p, a porosity n and a permeability k_p. The two-phase flow enters the cone at the inlet radius r_{in}, with a total mass flow rate $\dot{m}$ and a liquid mass ratio M. As fluid is drained out of the cone through powder and screen the fluid thickness h_f reaches the powder thickness h_p. The flow is then that of a powder matrix of thickness h_p the bottom of which is saturated with fluid over a thickness h_f, until all pores are emptied and a flow of damp powder is left. This flow of damp powder exits at the outlet radius r_{out}, as shown in Fig.5.

[Figure 6 about here.]

The objective is to solve for $h_f(r)$, $h_p(r)$, $u_f(r)$ and $u_p(r)$.

3 Dimensional analysis: Governing equations

The steady-state force equilibrium and mass conservation equations are established for the flow in each of the three regions A, B and C. Two models for flow behaviour in region A are discussed: in a first model the powder is assumed to have completely settled before it reaches the perforated part of the cone, while in a second model the input mixture (*slurry*) is still homogeneously mixed and the particles only settle because of the through-thickness flow velocity created by liquid seepage.

3.1 First model for region A: Layer of pure fluid flowing over a slipping layer of densely packed particles

In a first model for the flow in region A we consider the case where all the particles have settled onto the wall before entering the perforated basket. The flow at inlet is thus made of two distinct layers: a pure fluid layer flows on top of a slipping densely packed, saturated powder layer. We assume no slip at the interface between the layers, and the internal friction between powder particles is assumed to be larger than the shear traction at the interface between the two layers, so that all particles remain in the bottom layer. The average radial velocity of the powder is u_p and that of the fluid layer is u_f, as shown in Fig.3. The velocity profile of the layer thickness is assumed to be parabolic. The shear traction at the fluid/powder interface, τ_i, is in equilibrium with the weight per unit area of the fluid:

$$\tau_i = 3\mu \frac{u_f - u_p}{h_f - h_p} = \rho_f \left(h_f - h_p\right) r\Omega^2 \sin^2 \alpha \tag{7}$$

The shear traction at the powder/wall interface, τ, is in equilibrium with the weight per unit area of the saturated powder w_s and τ_i:

$$\tau = \left[\rho_p(1-n) + \rho_f n\right] h_p r\Omega^2 \sin^2 \alpha + \tau_i \tag{8}$$

As discussed earlier, the shear traction is represented by (1) where the effective pressure at the wall p reads

$$p_{eff} = r\Omega^2 \sin\alpha\cos\alpha\left[\rho_f\left(-\frac{h_s\left(h_f k_p - h_p k_s\right)}{h_s k_p + h_p k_s} + h_f - (1-n)h_p\right) + (1-n)\rho_p h_p\right] \quad (9)$$

The fluid inputs and outputs in an element of radial width dr are shown in Fig.7, where the internal and output seepage flow rates, Q_{Fip} and dQ_{oA} respectively, are calculated from Darcy's law as

$$Q_{Fip} = -2\pi\frac{k_p\rho_f\Omega^2\sin\alpha\cos\alpha}{\mu}r^2\frac{dh_f}{dr}h_p\sin\alpha\tan\alpha \quad (10)$$

$$dQ_{FoA} = \frac{2\pi k_p k_s r^2\Omega^2\left(h_f + h_s\right)\rho_f\cos\alpha\sin^2\alpha}{\mu\left(k_p h_s + h_p k_s\right)}dr \quad (11)$$

while the flow rate of fluid entering the control volume shown in Fig.7 via convective transport in the top layer $Q_{cf}(r)$ reads

$$Q_{Fcf}(r) = 2\pi r\left(h_f - h_p\right)u_f\sin\alpha \quad (12)$$

[Figure 7 about here.]

In the present analysis the internal seepage in the radial direction, Q_i, will be assumed negligible compared to the convective transport of fluid. We also note that (14) implies that, provided the powder porosity n is constant, the volumetric flow rate of fluid entering the element at r via the saturated powder layer Q_{Fcp} is equal to that leaving the element at $r+dr$. Upon making use of (11-12) fluid mass conservation in the control volume shown in Fig.7 then gives:

$$\frac{d\left[r\left(h_f - h_p\right)u_f\right]}{dr} + \frac{k_p k_s r^2\Omega^2\left(h_f + h_s\right)\rho_f\cos\alpha\sin\alpha}{\mu\left(k_p h_s + h_p k_s\right)} = 0 \quad (13)$$

Powder losses through the screen slots are neglected, in agreement with (Swindells 1982), so that powder conservation writes

$$h_p = \frac{N}{r u_p} \quad (14)$$

where $N \equiv \frac{(1-M)\dot{m}}{2\pi\rho_p(1-n)\sin\alpha}$. The mass flow rate of liquid at the inlet reads:

$$2\pi\rho_f r_{in}\left[(h_f - h_p)u_f + n h_p u_p\right]\sin\alpha = M\dot{m} \quad \text{at} \quad r = r_{in} \quad (15)$$

We then obtain a system of five equations (7, 8, 13, 14, 15) including an ODE (13) and its initial condition (15) for four unknowns (h_f, h_p, u_f, u_p).

3.2 Second model for region A: Simple settling

A second model is considered for region A, as shown in Fig.3. The particles are initially homogeneously dispersed in the fluid with a volumetric fluid ratio M_V and settle onto the wall because of the through-thickness fluid velocity due to fluid seepage. At r_{in} no particle is yet settled. In this model M_V is constant throughout the top layer in region A and is related to the initial liquid mass ratio M via

$$M_V = \frac{\rho_p M}{\rho_p M + \rho_f (1 - M)} \tag{16}$$

The density of the slurry is related to the densities of the slurry components and to its mass and volumetric liquid ratios via

$$\rho_s = M_V \rho_f + (1 - M_V)\, \rho_p = \frac{M_V \rho_f}{M} \tag{17}$$

The slurry viscosity μ_s is significantly higher owing to the presence of particles within the fluid, as discussed by (Oliver & Ward 1953) and (Rouillard & Koenig 1980). Relations (7, 8, 11, 14, 15) already obtained in §3.1 are somewhat modified by the new assumptions. We account for the change in density and viscosity of the top layer and re-write (7) as

$$\tau_i = 3\mu_s \frac{u_f - u_p}{h_f - h_p} = \rho_s\, (h_f - h_p)\, r\Omega^2 \sin^2 \alpha \tag{18}$$

The powder layer equilibrium relation (8) remains the same, provided that τ_i is now obtained from (18) and p_{eff} from:

$$p_{eff} = \frac{r\Omega^2 h_p \cos\alpha \sin\alpha \left[h_p k_s \left(n\rho_f + (1-n)\,\rho_p - \rho_t\right) + h_s \left((1-n)k_p\,(\rho_p - \rho_f) + \rho_f k_s\right) + \rho_t h_f k_s\right]}{h_s k_p + h_p k_s} \tag{19}$$

The volumetric flow rate of liquid entering the slurry layer at r in the element shown in Fig.7 is now

$$Q_{Fcf}(r) = 2\pi M_V r (h_f - h_p) u_f \sin\alpha \tag{20}$$

The liquid and the particles in the slurry layer have the same through-thickness velocity so that the physics of seepage as described earlier are not modified by the presence of particles

in the top layer. Seepage is however affected by the increase in density of the top layer: the hydrostatic pressure at the slurry/layer interface now writes $\rho_s g'(h_f - h_p)$ and (11) is consequently modified as follows:

$$dQ_{Fo} = \frac{2\pi k_p k_s r^2 \Omega^2 \sin^2\alpha \cos\alpha \left(\rho_f h_s + \rho_f h_p + \rho_s (h_f - h_p)\right)}{\mu \left(k_p h_s + h_p k_s\right)} dr \tag{21}$$

Upon making use of (20-21), (11) is modified into:

$$M_V \frac{d\left[r\left(h_f - h_p\right) u_f\right]}{dr} + \frac{dQ_{Fo}}{2\pi dr \sin\alpha} = 0 \tag{22}$$

[Figure 8 about here.]

Initial condition (15) is re-written as:

$$\dot{m} = 2\pi \rho_s r_{in} h_f u_f \sin\alpha \quad \text{at} \quad r = r_{in} \tag{23}$$

Along with (23) the other boundary condition is that no particles have settled at inlet, and we write this as

$$h_p = 0 \quad ; \quad r = r_{in} \tag{24}$$

The same approach as that previously used for fluid conservation is employed to obtain solid conservation within an element of width dr shown in Fig.8. The internal rate of transfer of particles between the slurry layer and the powder layer dQ_p when a flow rate of fluid dQ_{Fo} is drained out of the basket is

$$dQ_p = \frac{1 - M_V}{M_V} dQ_{Fo} \tag{25}$$

and powder volume conservation in the powder layer shown in Fig.8 yields

$$2\pi(1-n)\frac{d\left[r h_p u_p\right]}{dr} \sin\alpha = \frac{dQ_p}{dr} \tag{26}$$

and via (22,25-26) we obtain

$$(1-n)\frac{d\left[r h_p u_p\right]}{dr} = -(1 - M_V)\frac{d\left[r\left(h_f - h_p\right) u_f\right]}{dr} \tag{27}$$

Upon making use of (23-24) the ODE (27) is easily integrated into

$$\frac{(1-n)}{(1-M_V)} r h_p u_p = \frac{\dot{m}}{2\pi\rho_s \sin\alpha} - r\left(h_f - h_p\right) u_f \tag{28}$$

The problem still has thus the same structure as with Model 1: four unknowns (u_f, u_p, h_f, h_p) and a coupled system of three algebraic equations (8, 18, 28) and a first order ODEs (22) with the initial condition (23).

3.3 Region B: Saturated/Dry flow

The radius r_{CL1} marking the beginning of the colour line depends upon the model considered for region A, as does the thickness of the flow at this point, h_{CL1}. Once this initial condition is established however, the flow in the rest of the cone is independent of the choice of model for region A.

The section of the cone where the top layer is damp while the bottom of the flow is still saturated is now considered. A no slip condition between the layers is assumed, so that the whole flow slips on the wall at the same radial velocity $u_p(r)$.

3.3.0.1 Equilibrium and mass conservation The change in density due to fluid drainage out of the damp powder is neglected. As discussed earlier the friction at the wall is represented via (1), so that the equilibrium of the slender bi-phasic layer writes

$$a u_p + b p_{eff} = \left[\rho_p \left(1-n\right) h_p + \rho_f n h_f\right] r\Omega^2 \sin^2\alpha \tag{29}$$

where the effective pressure at the wall p_{eff} reads

$$p_{eff} = r\Omega^2 \sin\alpha\cos\alpha \left[n\rho_f h_f + (1-n)\rho_p h_p - \frac{\rho_f h_f h_s \left(k_p - k_s\right)}{h_f k_s + h_s k_p}\right] \tag{30}$$

(14) still holds as there is no loss of powder through the wall. The inlet velocity is given by the outlet velocity of the powder layer of the previous section, with $h_f = h_p = h_{CL1}$ at the colour line coordinate r_{CL1}.

3.3.0.2 Surface tension and seepage The change in pressure across the fluid surface due to surface tension can be estimated from Tabor's classical formula for capillaries (Tabor 1969) as $\delta P = \gamma/D$, where γ is the fluid surface tension and D the mean particle diameter.

The pressure drop driving the fluid through the powder is $\Delta p = \rho_f \Omega^2 r_{in} h_{in} \sin\alpha$, where r_{in} is the inlet radius of the cone and h_{in} is a reference layer thickness at inlet. In order to compare these pressure differences we introduce the surface tension number N_{ST} as

$$N_{ST} = \frac{\gamma}{D r_{in} h_{in} \rho \Omega^2 \sin\alpha} \tag{31}$$

For typical values N_{ST} is of the order of 10^{-2}, so that surface tension effects can be neglected and seepage still obeys Darcy's law in this configuration.

[Figure 9 about here.]

The elementary flow rate through the element of width dr at the coordinate r shown in Fig.9 is then

$$dQ_0 = \frac{2\pi\rho_f k_p k_s \left(h_f + h_s\right) \Omega^2 r^2 \cos\alpha \sin^2\alpha}{\mu \left(k_p h_s + h_f k_s\right)} dr \tag{32}$$

and internal transport of fluid via the layer radial displacement leads to the following convective volumetric flow rate:

$$Q_{Fcp}(r) = 2\pi n r h_f u_f \sin\alpha \tag{33}$$

Fluid conservation in the element of the bottom layer shown in Fig.9 then yields the ODE

$$\frac{d\left[r h_f u_p\right]}{dr} + \frac{\rho_f k_p k_s \left(h_f + h_s\right) \Omega^2 r^2 \cos\alpha \sin\alpha}{\mu \left(k_p h_s + h_f k_s\right)} = 0 \tag{34}$$

3.4 Region C: After the colour line, flow of damp powder

In region C the pores are all filled with air and a film of fluid coats the particles. Drainage still occurs which regenerates the basal liquid film, so that the coefficient a in (1) is taken as constant. As discussed earlier the value of a in this region should be lower than that used in regions A and B but for simplicity it will not be changed. Not that this simplification does not affect the position of the colour line as estimated by this model. The dry friction coefficient b does not change either. The flow is now entirely controlled by the equilibrium between the basal shear traction and the centrifugal traction:

$$a u_p + b p_{eff} = \rho_p \left(1 - n\right) r h_p \Omega^2 \sin^2\alpha \tag{35}$$

where the effective pressure at the wall p_{eff} reads

$$p_{eff} = \rho_p (1-n) r h_p \Omega^2 \cos\alpha \sin\alpha \tag{36}$$

(14,35-36) lead to an algebraic equation for h_p and u_p,

$$h_p = \frac{1}{r\Omega \sin\alpha} \left(\frac{aN}{\left(1-\hat{b}\right)(1-n)\rho_p} \right)^{1/2} \tag{37}$$

$$u_p = \Omega \sin\alpha \left(\frac{N\left(1-\hat{b}\right)(1-n)\rho_p}{a} \right)^{1/2} \tag{38}$$

Note the the flow velocity u_p is independent of position r in region C.

4 Non-dimensional approach

The inlet values of relations (37-38) are used in order to non-dimensionalize the above analysis. We obtain

$$h_{ref} \equiv \frac{1}{r_{in}\Omega \sin\alpha} \left(\frac{aN}{\left(1-\hat{b}\right)(1-n)\rho_p} \right)^{1/2} \tag{39}$$

$$u_{ref} \equiv \Omega \sin\alpha \left(\frac{N\left(1-\hat{b}\right)(1-n)\rho_p}{a} \right)^{1/2} \tag{40}$$

Upon making use of (39-40) we define the following dimensionless groups:

(i) the radial coordinate

$$R \equiv \frac{r}{r_{in}} \tag{41}$$

(ii) the dimensionless screen thickness H_s

$$H_s \equiv \frac{h_s}{h_{ref}} \tag{42}$$

(iii) the dimensionless fluid thickness H_f

$$H_f \equiv \frac{h_f}{h_{ref}} \tag{43}$$

(iv) the dimensionless powder thickness H_p

$$H_p \equiv \frac{h_p}{h_{ref}} \tag{44}$$

(v) the dimensionless fluid velocity U_f

$$U_f \equiv \frac{u_f}{u_{ref}} \tag{45}$$

(vi) the dimensionless powder velocity U_p

$$U_p \equiv \frac{u_p}{u_{ref}} \tag{46}$$

(vii) the slenderness ratio $\hat{H}$

$$\hat{H} \equiv \frac{h_{ref}}{r_{in}} \cot \alpha \tag{47}$$

Note the for the slender flow result to hold $\hat{H}$ must be significantly smaller than unity (Bizard et al. 2010)

(viii) the density ratio $\overline{\rho}$, which will always be larger than unity in this analysis,

$$\overline{\rho} \equiv \frac{\rho_p}{\rho_f} \tag{48}$$

(ix) the viscosity number $\hat{\mu}$

$$\hat{\mu} \equiv \frac{a h_{ref}}{3 \mu \chi} \tag{49}$$

where $\chi = (1-n)\left(1-\hat{b}\right)\overline{\rho}$

(x) the seepage number S,

$$S \equiv \frac{k_s \rho_f \Omega^2 r_{in}^2 \sin \alpha \cos \alpha}{\mu h_{ref} u_{ref}} \tag{50}$$

(xi) the permeability ratio κ

$$\kappa \equiv \frac{k_s}{k_p} \tag{51}$$

(xii) Following (Rouillard & Koenig 1980) we define the relative viscosity of the slurry as:

$$\overline{\mu} \equiv \frac{\mu_s}{\mu} \tag{52}$$

Upon using (39-52) we can re-write the governing equations for each region of the cone.

4.1 Region A - Model 1

Fluid equilibrium (7)

$$(U_f - U_p) - \hat{\mu} R \left(H_f - H_p\right)^2 = 0 \tag{53}$$

Solid equilibrium (8)

$$\begin{aligned} &\hat{\mu} H_f \left[-H_p \left(R H_s (\hat{b}\kappa - \xi) + \kappa \chi U_p \right) + R\kappa(\hat{b} + \xi) H_p^2 - \chi H_s U_p \right] \\ &- \hat{b} R \kappa \hat{\mu} H_f^2 H_p + \hat{\mu} H_p^2 \left(R H_s (\hat{b}\kappa - \xi) + \kappa \chi U_p \right) \\ &+ H_p \left(\kappa U_f + U_p \left(\hat{\mu} \chi H_s - \kappa \right) \right) + H_s \left(U_f - U_p \right) - R\kappa\hat{\mu}\xi H_p^3 = 0 \end{aligned} \tag{54}$$

where $\xi \equiv \hat{b}(1-n) + n + \chi$

Fluid conservation (13)

$$\frac{S R^2 \left(H_f + H_s\right)}{\kappa H_p + H_s} + \frac{d\left[R \left(H_f - H_p\right) U_f\right]}{dR} = 0 \tag{55}$$

Solid conservation (14)

$$R H_p U_p = 1 \tag{56}$$

Initial condition (15)

$$(H_f - H_p) U_f + n H_p U_p = \frac{M(1-n)}{1-M} \tag{57}$$

Region A ends when $H_f = H_p$, at the dimensionless coordinate $R = R_{CL1}$.

4.2 Region A - Model 2

Fluid equilibrium (18)

$$(U_f - U_p) - \frac{\hat{\mu} M_V}{\overline{\mu} M} R\,(H_f - H_p)^2 = 0 \tag{58}$$

Solid equilibrium (8)

$$\frac{\hat{b} R H_p \Big((\hat{b}-1) M_V \kappa H_f + \kappa H_p (\hat{b}(M - M_V) - M\xi + M_V) + M H_s ((\hat{b}-1)\kappa - \xi + 1) \Big)}{(\hat{b}-1) M\,(\kappa H_p + H_s)}$$
$$- \frac{R(\hat{b} - \xi) H_p}{\hat{b} - 1} + \frac{\overline{\mu}\,(U_p - U_f)}{\hat{\mu}\,(H_f - H_p)} + \chi U_p = 0 \tag{59}$$

Fluid mass conservation (22)

$$\frac{S R^2\,(M_V H_f + H_p (M - M_V) + M H_s)}{M M_V\,(\kappa H_p + H_s)} + \frac{d\,[R\,(H_f - H_p)\,U_f]}{dR} = 0 \tag{60}$$

Solid mass conservation (26)

$$(1 - M_V) R\,(H_f - H_p)\,U_f$$
$$+ R H_p (1 - n) U_p = \overline{\rho} \frac{M (1 - M_V)(1 - n)}{M_V (1 - M)} \tag{61}$$

Total mass flow rate at inlet (23)

$$U_f H_f = \frac{M (1 - n) \overline{\rho}}{(1 - M) M_V} \quad ; \quad R = 1 \tag{62}$$

Initial solid thickness (24)

$$H_p = 0 \quad ; \quad R = 1 \tag{63}$$

4.3 Region B

Layer equilibrium (29)

$$H_f \Big(R H_s (\hat{b}\kappa - \xi + \chi) - R\kappa\chi H_p + \kappa\chi U_p \Big) + R\kappa H_f^2 (\hat{b} - \xi + \chi) + \chi H_s\,(U_p - R H_p) = 0 \tag{64}$$

Fluid conservation (34)

$$\frac{SR^2\left(H_f+H_s\right)}{n\left(\kappa H_f+H_s\right)}+\frac{d\left[RH_fU_p\right]}{dR}=0 \tag{65}$$

Solid mass conservation (56) still holds. Region B ends at $R=R_{CL2}$, when $H_f=0$

4.4 Region C

Upon making use of (37-41) we obtain the algebraic equations for H_p and U as

$$H_p=\frac{1}{R} \tag{66}$$

$$U_p=1 \tag{67}$$

respectively.

5 Numerical results

5.0.0.3 Numerical values The following typical values will be used throughout this paper for numerical illustrations:

$$\begin{aligned}
&\mu=5\text{Pa.s} \quad ; \quad r_{in}=0.54\text{m} \quad ; \quad \alpha=30^\circ \quad ; \quad \Omega=2200\text{RPM} \quad ; \quad \dot{m}=8\text{TPH}\\
&M=50\% \quad ; \quad n=0.4 \quad ; \quad \rho_p=1500\text{kg m}^{-3} \quad ; \quad \rho_f=1400\text{kg m}^{-3} \quad ; \quad \gamma=50\text{mN m}^{-1}\\
&k_p=10^{-10}\text{m}^2 \quad ; \quad a=8\times10^4 \quad ; \quad b=0.5 \quad ; \quad h_s=300\times10^{-6}\text{m} \quad ; \quad k_s=6.1\times10^{-11}\text{m}^2\\
&\mu_s=500\text{Pa.s}
\end{aligned} \tag{68}$$

For these values $u_{ref}=0.08\text{m s}^{-1}$ and $h_{ref}=8.2mm$. The dimensionless groups have the following values:

$$\begin{aligned}
&\overline{\rho}=1.07 \quad ; \quad P=0.21 \quad ; \quad \hat{H}=2.6\times10^{-2} \quad ; \quad \hat{\mu}=131\\
&S=6.0\times10^{-5} \quad ; \quad \kappa=0.12 \quad ; \quad \overline{\mu}=100 \quad ; \quad H_s=0.018
\end{aligned} \tag{69}$$

The solution to the systems of equations presented earlier for each model is found numerically making use of the *NDSolve* function of Mathematica (Wolfram Research n.d.). While the initial conditions are significantly different, both models display a similar behaviour at the colour line, as shown in Fig.11. The powder thickness increases sharply at the colour line, and we interpret this as follows. The diminution in fluid content reduces buoyancy

and consequently increases the basal friction via the Coulomb friction term of (1), which slows the flow down and increases significantly the thickness of the flowing damp powder. Note that for the set of data used, which is typical of an industrial low-grade continuous conical centrifuge, the reference velocity u_{ref} is of the same order as measured by Swindells (Swindells 1982) in his experiments.

The sensitivity of the colour line end position, R_{CL2}, to key dimensionless parameters is now explored. Firstly, note that not all dimensionless groups defined earlier appear in the governing equations (7-67). In particular, the slenderness ratio $\hat{H}$, the Reynolds number P and the cone angle α do not influence the position of the color line when all other dimensionless parameters are held constant. For model 1, the change ΔR_{CL2} of R_{CL2} when a parameter X is changed by ΔX is given by

$$\frac{\Delta R_{CL2}}{R_{CL2}} = -1.2\frac{\Delta S}{S} + 0.5\frac{\Delta M}{M} + 0.2\frac{\Delta \hat{b}}{\hat{b}} + 0.1\frac{\Delta \kappa}{\kappa} + 3\times 10^{-2}\frac{\Delta H_s}{H_s} - 3\times 10^{-2}\frac{\Delta n}{n} \quad (70)$$

For model 2, this sensitivity analysis gives

$$\frac{\Delta R_{CL2}}{R_{CL2}} = -1.2\frac{\Delta S}{S} + 0.3\frac{\Delta M}{M} + 0.2\frac{\Delta \hat{b}}{\hat{b}} + 0.1\frac{\Delta \kappa}{\kappa} + 0.1\frac{\Delta n}{n} + 4\times 10^{-2}\frac{\Delta H_s}{H_s} - 10^{-2}\frac{\Delta \overline{\mu}}{\overline{\mu}} \quad (71)$$

$(\hat{\mu}, \overline{\rho})$ have very little influence on the colour line position. We note that the only parameter that differs between the two models, $\overline{\mu}$, has a very mild influence on the colour line in model 2. We conclude that the constitutive model chosen for the slurry is sufficient for this analysis, and that chosing a power-law constitutive model, as proposed by (Swindells 1982), only adds unnecessary complication. The apparent importance of the initial fluid mass ratio M is relative: its amplitude can only vary within a small range as the input material can not be fed below saturation. Practically, M is thus constrained to lie between $n\rho_f/\left[n\rho_f + (1-n)\rho_p\right]$ and 1. For the practical values (68) the lower bound is about 0.4.

[Figure 10 about here.]

[Figure 11 about here.]

[Figure 12 about here.]

[Figure 13 about here.]

5.1 Maximizing the residence time

The residence time in region C t_C is the ratio of the length of region C to the flow velocity in this region u_{ref}:

$$t_C = \frac{R_{out} - R_{CL2}}{\Omega \sin \alpha} \sqrt{\frac{3\overline{\rho}\hat{\mu}}{P\hat{H} \tan \alpha}} \tag{72}$$

5.2 Optimization

In order to optimize a conical centrifugal filter the two quantities t_C and N_{CAP} should be maximized. This can be achieved by changing the design of the machine or its operating conditions, via the dimensionless groups (41-52). We note first that some dimensionless groups can not be modified, such as the density ratio $\overline{\rho}$. Examination of (41) then shows that modifying the magnitude of some groups ($\hat{H}$, $\hat{\mu}$, $\tan \alpha$) will modify significantly N_{CAP} but only mildly affect the residence time t_C. Finally, it is clear from the previous results and (72) that increasing S is beneficial to both the residence time and the drying efficiency.

6 Concluding remarks

This paper provides a framework for the analysis of drying flow of wet granular material in a conical centrifugal filter. A one dimensional model of the steady state axisymmetric flow in a spinning perforated cone has been developed. While the screen resistance to seepage has not been considered, it is argued that it does not change relative influence of the non-dimensional groups identified here. Upon making use of the presented relations it is possible to assess the influence of a change in operating parameters on the performance of a machine. Another application of these results is the development of a continuous conical centrifuge for a new product. Such a development would only require the knowledge of easily measurable quantities such as the Coulomb friction coefficient of the solid against the wall, its density and that of the fluid.

7 Acknowledgements

The authors are grateful to the Ashby Scholarship Fund, the Cambridge European Trust and Peterhouse for financial support.

References

Bizard, A., Symons, D. & Fleck, N. (2010), 'Flow of damp powder in a rotating impervious cone', *JAM* .

Dombrowski, H. S. & Brownell, L. E. (1954), 'Residual equilibrium saturation of porous media', *Industrial and Engineering Chemistry* **46**(6), 1207–1219. Times Cited: 63.

Greig, C. (1995), Studies on continuous sugar centrifuges, PhD thesis.

Makarytchev, S. V., Xue, E., Langrish, T. A. G. & Prince, R. G. H. (1997), 'On modelling fluid flow over a rotating conical surface', *Chemical Engineering Science* **52**(6), 1055–1057.

Oliver, D. R. & Ward, S. G. (1953), 'Relationship between relative viscosity and volume concentration of stable suspensions of spherical particles', *Nature* **171**(4348), 396–397.

Rouillard, E. & Koenig, M. (1980), 'The viscosity of molasses and massecuite', *Proceedings of The South African Sugar Technologists' Association* pp. 89–92.

Swindells, R. (1982), A mathematical model of a continuous sugar centrifuge, PhD thesis.

Tabor, D. (1969), *Gases, liquids and solids*, Penguin, Harmondsworth,. [by] D. Tabor. illus. 21 cm.

Wolfram Research, I. (n.d.), 'Mathematica 5.0'.

Yilmazer, U. & Kalyon, D. M. (1989), 'Slip effects in capillary and parallel disk torsional flows of highly filled suspensions', *Journal of Rheology* **33**(8), 1197–1212.

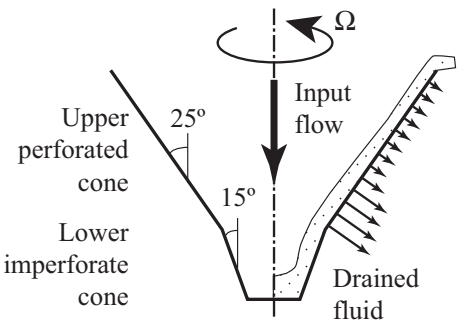

Figure 1: Section of a typical sugar conical continuous centrifuge

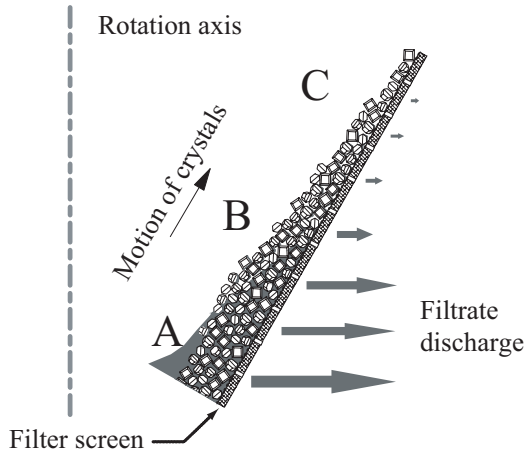

Figure 2: Flow in a rotating perforated cone

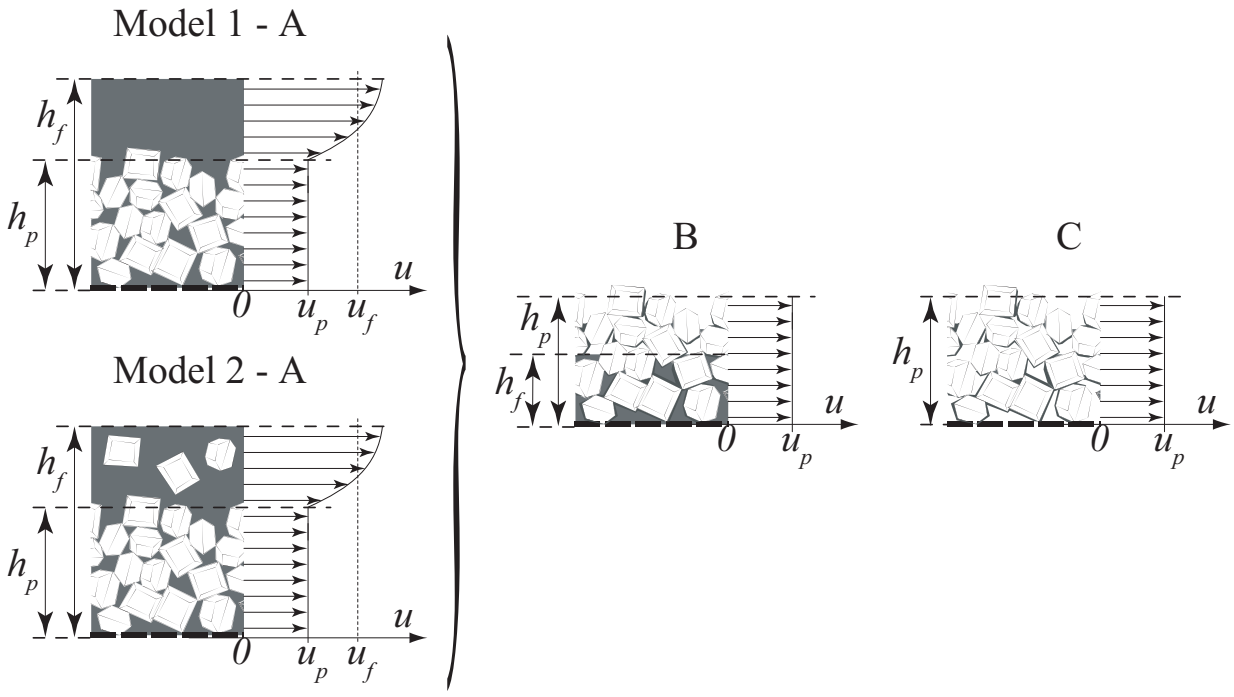

Figure 3: Microstructure and velocity profile of the solid/liquid/air phases in regions A, B and C

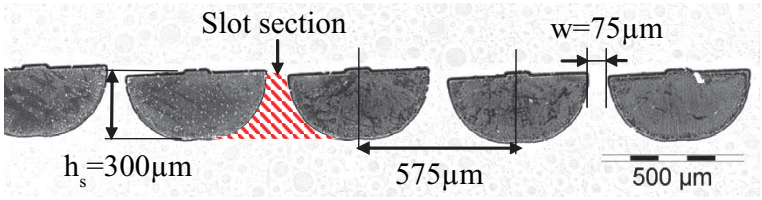

Figure 4: Section of a typical sugar centrifuge screen

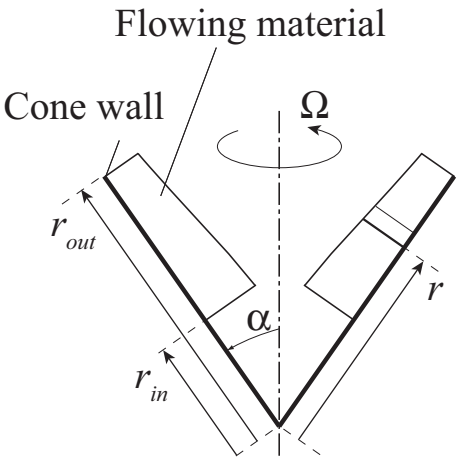

Figure 5: Cone geometry

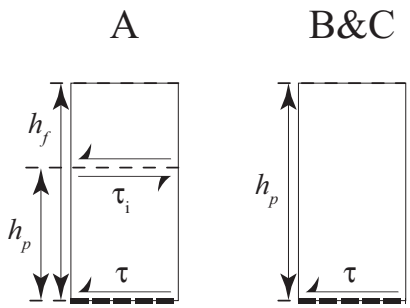

Figure 6: Equilibrium in regions A, B and C

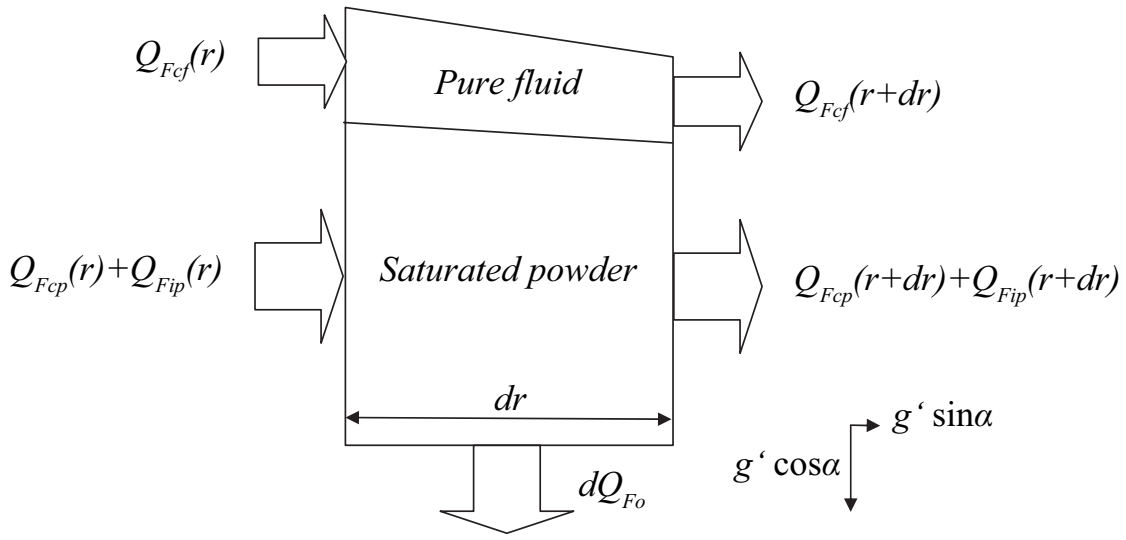

Figure 7: Model 1 - Region A: Fluid volume conservation through a control volume of width $2\pi r \sin\alpha$ and length dr subjected to a local gravity of amplitude $g' = r\Omega^2 \sin\alpha$)

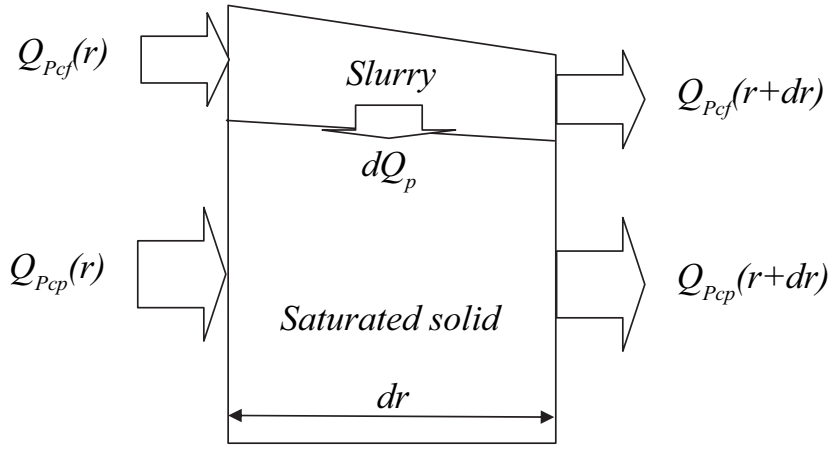

Figure 8: Model2 - Region A: Solid conservation with settling

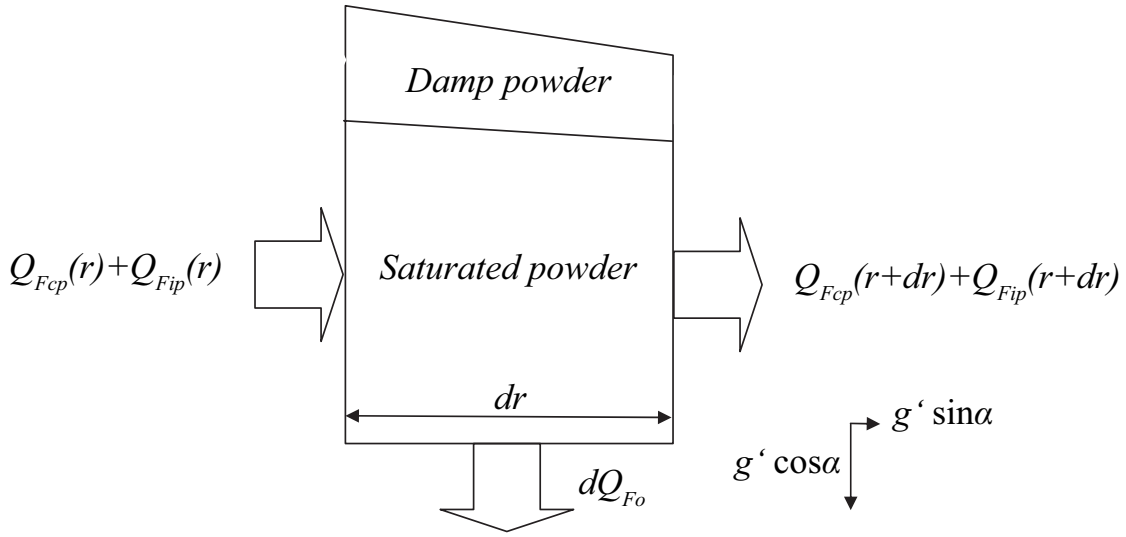

Figure 9: Region B: Fluid volume conservation through a control volume of width $2\pi r \sin\alpha$ and length dr subjected to a local gravity of amplitude $g' = r\Omega^2 \sin\alpha$ within the colour line region ($h_f < h_p$)

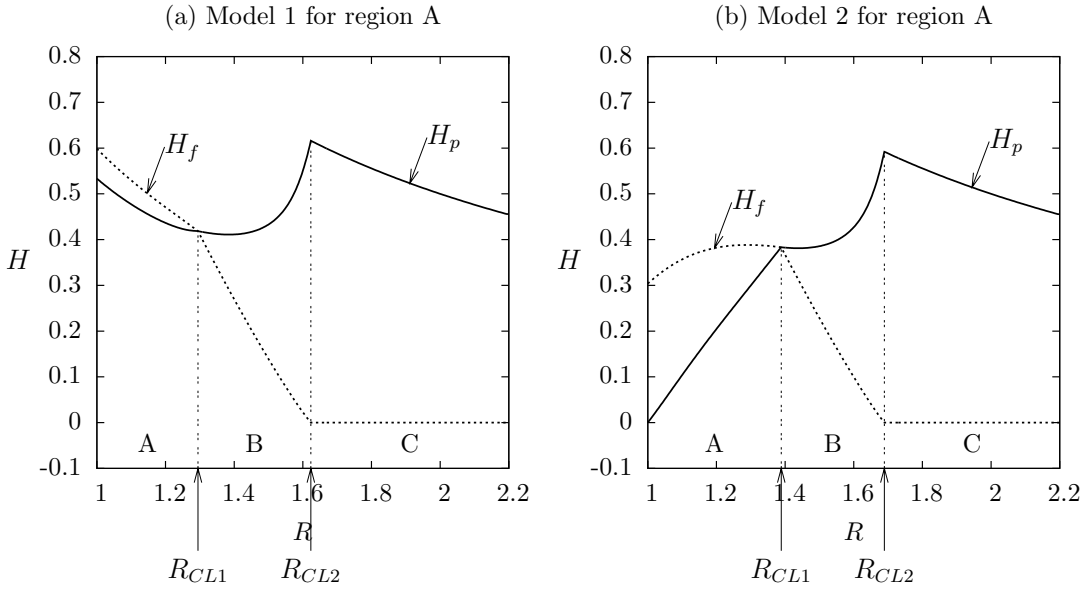

Figure 10: Typical solutions of the three systems of equations for H_f and H_p within the entire cone for the typical values given in (68) for (a) Model 1 and (b) Model 2 of region A

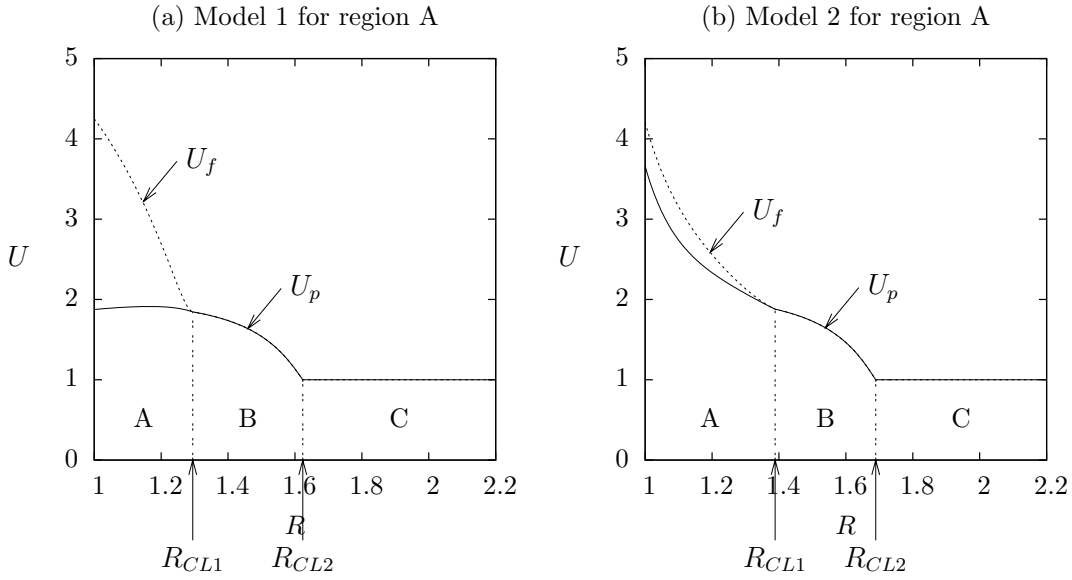

Figure 11: Typical solutions of the three systems of equations for U_f and U_p within the entire cone for the typical values given in (68) for (a) Model 1 and (b) Model 2 of region A

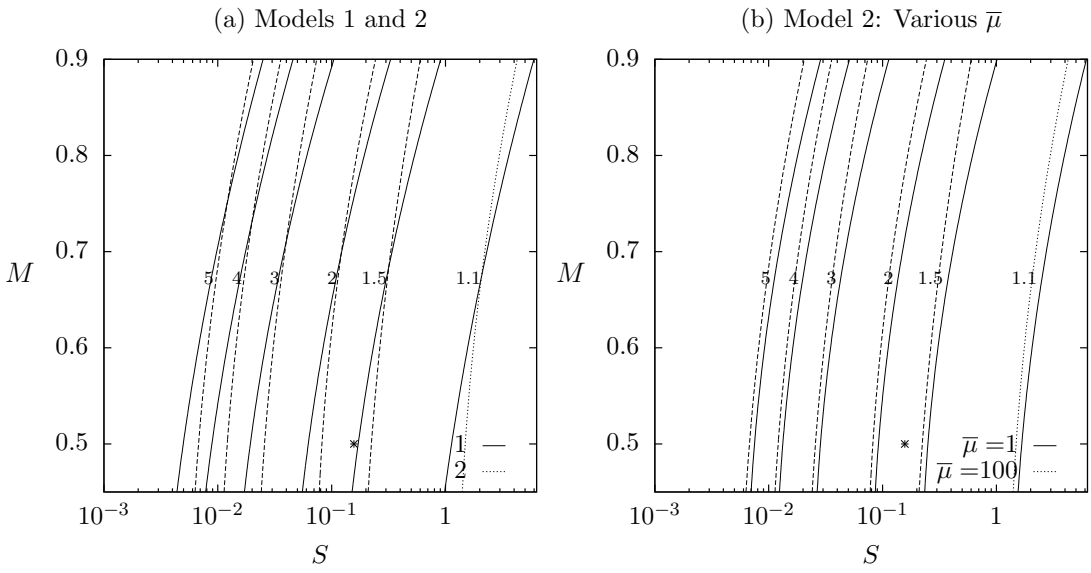

Figure 12: R_{CL2} contours in the (S, M) plane for the typical values given in (68) for models 1 and 2

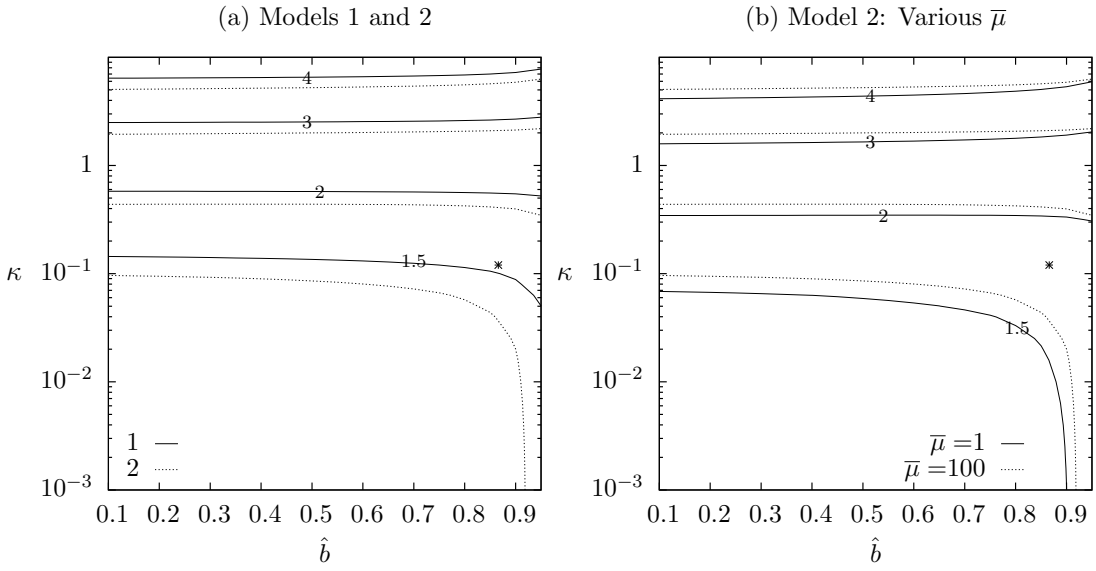

Figure 13: R_{CL2} contours in the ($\hat{b}$, κ) plane for the typical values given in (68) for models 1 and 2